

Current-driven domain wall dynamics in ferrimagnetic Ni-doped Mn_4N films : very large domain wall velocities and reversal of motion direction across the magnetic compensation point

Sambit Ghosh,^{†,‡} Taro Komori,[‡] Ali Hallal,[†] Jose Peña Garcia,[¶] Toshiki Gushi,^{‡,†}
Taku Hirose,[‡] Haruka Mitarai,[‡] Hanako Okuno,[§] Jan Vogel,[¶] Mairbek Chshiev,[†]
Jean-Philippe Attané,[†] Laurent Vila,^{*,†} Takashi Suemasu,[‡] and Stefania
Pizzini^{*,¶}

[†]*Univ. Grenoble Alpes, CEA, CNRS, Grenoble INP, IRIG-Spintec, 38054 Grenoble, France*

[‡]*Institute of Applied Physics, Graduate School of Pure and Applied Sciences, University of
Tsukuba, Tsukuba, Ibaraki 305-8573, Japan*

[¶]*Univ. Grenoble Alpes, CNRS, Institut Néel, 38042 Grenoble, France*

[§]*Univ. Grenoble Alpes, CEA, IRIG-MEM, 38000 Grenoble, France*

E-mail: laurent.vila@cea.fr; stefania.pizzini@neel.cnrs.fr

Abstract

Spin-transfer torque (STT) and spin-orbit torque (SOT) are spintronic phenomena allowing magnetization manipulation using electrical currents. Beyond their fundamental interest, they allow developing new classes of magnetic memories and logic devices, in particular based on domain wall (DW) motion. In this work, we report the study of STT driven DW motion in ferrimagnetic manganese nickel nitride ($\text{Mn}_{4-x}\text{Ni}_x\text{N}$)

films, in which a fine adjustment of the Ni content allows setting the magnetic compensation at room temperature. The reduced magnetization, combined with the large spin polarization of conduction electrons, strongly enhances the STT so that domain wall velocities approaching 3000 m/s can be obtained for Ni compositions close to the compensation point. In addition, a reversal of the domain wall motion direction is observed when the magnetic compensation composition is crossed. This striking feature, related to the change of direction of the spin polarization with respect to that of the net magnetization, is clarified by *ab initio* band structure calculations.

Introduction

Domain walls (DWs) separate magnetic domains present in ferromagnetic materials. Current-driven DW motion was predicted theoretically by Berger in 1978¹ and then extensively studied for its potential applications in domain wall racetrack memories², DW MRAM³, spin torque majority gate^{4,5} and other domain-wall-based logic devices⁶⁻⁹. The two mechanisms leading to DW motion driven by spin polarized currents are the spin-transfer torque (STT) and the spin orbit torque associated to the spin Hall effect (SHE-SOT)¹⁰. While in the case of STT the charge current is spin polarized within the ferromagnetic layer by *sd* exchange interaction¹¹⁻¹³, in the case of SHE-SOT, the spin polarized current is generated by SHE in a neighbouring film (Pt, W, Ta ..), and then injected into the ferromagnetic layer¹⁴⁻¹⁷, resulting in both cases into a torque applied on the DWs.

Studies on systems in which domain walls are driven by STT are nowadays rare, mainly because there are practically no reports of efficient STT in thin films with perpendicular magnetization. In the last decade the interest of the spintronic community has focused on thin ferromagnetic films deposited on a heavy metal, where the interfacial Dzyaloshinskii-Moriya interaction (DMI) stabilizes chiral Néel walls that can be efficiently driven by SHE-SOT^{16,17}.

Recently, current-induced magnetization dynamics in ferrimagnets has become a wide

field of research. In these materials, two magnetic sub-lattices are anti-ferromagnetically coupled, and the compensation of magnetic (and angular) moment of the two sublattices may be obtained by varying either the temperature or the composition of the material. Previous experiments on ferrimagnets¹⁸⁻²¹, mostly carried out on thin films deposited on a heavy metal, have evidenced new physical mechanisms taking place in the vicinity of these compensation points, leading to large SOT-driven DW velocities^{18,19}.

In the present work we report the study of ferrimagnetic Mn_4N thin films doped with Ni, where a fine tuning of the Ni atomic content allows setting the magnetic compensation point close to room temperature. In these films, neither bulk nor interfacial DMI are present; domain walls have then a Bloch internal structure and are driven by STT. Our Kerr microscopy measurements show that thanks to the large spin polarization of the conduction electrons and to the low spontaneous magnetization close to the compensation point, domain walls can be moved by STT with an unprecedented efficiency. Interestingly, a remarkable reversal of the DW motion direction is observed when the Ni compensation composition is crossed. This striking feature, related to the change of direction of the spin polarization with respect to that of the net magnetization, is explained by the results of band structure calculations.

Structural, magnetic and transport properties

Ferrimagnetic Mn_4N grows with a tetragonal anti-perovskite crystal structure (Fig. 1a), with two types of Mn atoms at the corner (site I) and at the face centred sites (site II). The two magnetic sublattices are anti-ferromagnetically coupled, with the net magnetization parallel to the Mn(I) moment. With a high Curie temperature of 745K²²⁻²⁵, a low magnetization (around 70-150 kA/m), and a relatively high uniaxial perpendicular anisotropy (0.1×10^6 MJ/m³)²⁶⁻³¹, this rare-earth free material is an interesting candidate for spintronic applications.

Using either pulsed-laser deposition²⁹, DC reactive sputtering²⁸ or molecular beam epi-

taxy^{27,30}, Mn₄N thin films can be grown on different substrates such as Si²⁶, SiC and GaN³², MgO²⁷⁻³¹, SrTiO₃ (STO)^{27,31,33} and (LaAlO₃)_{0.3}(Sr₂TaAlO₆)_{0.7} (LSAT)³⁴. Mn₄N films deposited on STO(001) were shown to exhibit smooth magnetic domains (at the mm scale), due to a reduced density of pinning sites³³, and record current-induced domain wall velocities driven by STT (900 m/s for J=1.3 TA/m²)³⁵.

In this paper, we focus on Ni-doped Mn₄N thin films epitaxially grown on STO(001) substrates³⁶. 10 nm and 30 nm thick Mn_{4-x}Ni_xN films, with nominal x varying between 0.1 and 0.25, were grown by molecular beam epitaxy on STO(001) substrates and capped with a 3 nm thick SiO₂ layer. Transmission electron microscopy (TEM), reflection high-energy electron diffraction and X-ray diffraction measurements were performed to check their crystalline quality. The high resolution TEM micrograph of a 30 nm thick Mn_{3.75}Ni_{0.25}N film shown in Fig. 1b illustrates a highly ordered crystalline structure, with a negligible density of defects. The high-angle annular dark field scanning transmission electron microscopy (HAADF-STEM) image of the full stack and the elemental maps of Mn, O and Ni obtained by energy-dispersive X-ray spectroscopy (EDX), are shown in Fig. 1c-f. These data demonstrate that the distribution of the Ni atoms throughout the film has a good uniformity. On the other hand, while oxygen is mostly concentrated in the substrate and in the capping layer, a small region of the film, at the interface with the capping layer, appears to be oxidized. This layer has to be considered as a magnetically dead layer.

Our previous X-ray magnetic circular dichroism (XMCD) measurements³⁶ showed that Ni occupies preferentially the Mn(I) sites of Mn₄N. Since the moment carried by Ni atoms is anti-parallel to that of Mn(I), increasing the Ni atomic content allows reducing the overall magnetization. Beyond a critical Ni content, the net magnetization direction is thus expected to reverse with respect to the original one, i.e. to become anti-parallel to the Mn(I) magnetization. An analytical calculation of M_s using the magnetic moments of Mn(I), Mn(II) and Ni atoms extracted from neutron diffraction measurements^{22,25} predicts the magnetization compensation to occur for $x = 0.18$, corresponding to 3.6 at% of Ni. The presence

of a compensation point around this Ni content was proved by XMCD measurements and confirmed by the sign reversal of the anomalous Hall angle for samples with Ni content on either side of it³⁷. The effect of the substitution of Mn(I) atoms with Ni atoms on the net magnetization is sketched in Fig. 1a: the net magnetization is parallel to the Mn(I) moment below the compensation point ($x = 0, 0.12$) and becomes parallel to the Mn(II) moment above it ($x = 0.25$).

The anomalous Hall effect (AHE) curves measured for $\text{Mn}_{4-x}\text{Ni}_x\text{N}$ films patterned into Hall crosses and Van der Pauw method on blanket layers are shown in Fig. 2a as a function of the Ni concentration ($x = 0, 0.15, 0.2$ and 0.25). The sharp magnetization switching observed for all the films reveals that they retain the large perpendicular magnetic anisotropy after patterning. A switch of the AHE angle from negative to positive is observed for Ni content between $x = 0.15$ and $x = 0.2$. This indicates that the net magnetization changes direction between these two values, confirming the previously obtained compensation composition for $x \approx 0.18$.

Fig. 2b shows the variation of the spontaneous magnetization M_s as a function of the Ni content, measured by vibrating sample magnetometry (VSM-SQUID) at room temperature. For each sample, the direction of the net magnetization is deduced from the sign of the AHE angle (as in Fig. 2a): positive/negative sign of M_s in the Fig. 2b indicates net magnetization parallel/anti-parallel to the Mn(I) magnetic moment. In agreement with previous results^{36,37}, M_s is observed to decrease with increasing Ni content and to change direction for x between 0.15 and 0.2. Note that for the nominal Ni content $x = 0.15$, a difference in the net magnetization direction is observed between the 10 nm and 30 nm thick films. This might be due to a small deviation from the targeted 3 at% of Ni content in the two films. For this reason, in Fig. 2b the shaded area indicates the deviation from the nominal Ni content x at the compensation point observed in this series of samples.

Domain wall dynamics

The dynamics of domain walls in the $\text{Mn}_{4-x}\text{Ni}_x\text{N}$ films was studied using polar magneto-optical Kerr effect (MOKE) microscopy, with differential imaging to enhance the magnetic contrast. Samples were patterned into micrometric strips using electron beam lithography. The image of a complete device is shown in Fig. 3a (see Methods for more details). Fig. 3b shows differential MOKE images in which the black and white contrasts represent the displacement of the domain walls along the nanowires, during the application of current pulses. As expected for STT-driven DW motion, for a given current polarity all the DWs move in the same direction. The limited dispersion of the DW displacements among the nanowires points out that DWs are weakly pinned by defects.

Fig. 3c shows the average DW velocities versus current density J , measured for samples with Ni content on both sides of the compensation point. These are compared with the velocity measured for the undoped Mn_4N sample already reported in Ref.³⁵, for which the net magnetization is the largest ($M_s = +71$ kA/m). For compositions below the compensation point, the DWs move parallel to the direction of the electron flow and their mobility (dv/dJ) increases as the net magnetization decreases (*i.e.* as the Ni concentration increases). When the compensation point is crossed, the DWs reverse their direction of motion.

Furthermore very large velocities parallel to the current flow, approaching 3000 m/s, are obtained for a Ni content around $x = 0.25$ ($M_s \approx -20$ kA/m) with a current density $J = 1.2 \times 10^{12}$ A/m². The corresponding DW mobility ($m = \approx 20 \times 10^{-10} \text{m}^3\text{C}^{-1}$) exceeds the largest SOT-driven DW mobility measured in ferrimagnetic GdCo/Pt thin films ($6 \times 10^{-10} \text{m}^3\text{C}^{-1}$, obtained close to the angular momentum compensation point, at 250K¹⁹). Away from the compensation point the DW mobility decreases and reaches values similar to those obtained for Mn_4N .

In Fig. 3d the domain wall velocities obtained for the various films using current density $J = 1 \times 10^{12}$ A/m², are plotted as a function of the net magnetization M_s . A clear divergence of the DW velocity is observed when the magnetic compensation point is approached.

In order to explain these results, let us summarize the predictions of the 1D model for STT-driven domain wall motion (see also Ref. ³⁵). In thin films with out-of-plane magnetization and in the adiabatic limit, a DW may move continuously only when its magnetization can start precessing in order to align with the spin polarization of the incoming conduction electrons^{38,39}. To do so, the DW energy has to overcome the demagnetizing energy K_D given by the difference in energy between the Bloch and the Néel DW configurations. This gives rise to an intrinsic critical current density J_c above which the DW starts moving. To explain the experimental results obtained for in-plane magnetized films, where DWs were observed to move for current densities below the calculated J_c , a non-adiabatic contribution to the torque was introduced^{38,40}, characterized by a dimensionless parameter β . This term, acting as an effective magnetic field, allows for the DW to move in a steady state regime below J_c , resulting in the disappearing of the intrinsic threshold current. Well above J_c , the domain wall moves in a precessional regime with a velocity given by^{38,39}:

$$v = \frac{1 + \alpha\beta}{1 + \alpha^2}u \quad (1)$$

where:

$$u = \frac{g\mu_B}{2eM_s}PJ \quad (2)$$

is the spin drift velocity, with α , P , g , μ_B and e indicate the Gilbert damping parameter, the spin polarization of the current, the Landé factor, the Bohr magneton and the electron charge, respectively.

In the films studied in this work, the saturation magnetization is very small, so that the demagnetizing energy in all the films is negligible, leading to a very low J_c of the order of 2×10^{10} A/m² for Mn₄N³⁵. This current density is much lower than that for which DWs are observed to move in our samples (e.g. 9×10^{10} A/m² for $x=0.2$ and 3.5×10^{11} A/m² for $x=0.15$). For this reason, the adiabatic term is sufficient to explain the domain wall motion

in our systems. Even assuming that the non adiabatic term contributes to the DW dynamics with $\beta = 4\alpha$, (i.e. the maximum β measured for systems with out-of-plane magnetization⁴¹), using $\alpha = 0.15$ measured for Mn_4N , this should not represent more than 10% of the measured velocity.

Equations 1 and 2 show that the domain wall mobility is expected to change linearly with the ratio P/M_s . For a given spin polarization, the DW velocity is expected to increase when the magnetization compensation is approached, as M_s reduces, in agreement with the experimental results. In principle, through equations 1 and 2, the measured domain wall mobility should allow us to obtain the value of the spin polarization. However, the relatively large error bars associated to the measured values of M_s and α does not allow us to quantitatively evaluate the variation of the spin polarization versus the Ni concentration. Nevertheless, all the measured velocities fall within shaded area in Fig. 3d, that delimits the DW velocities calculated with Eq. 1 setting $0.3 < P < 0.9$ and using $\alpha = 0.15$, $\beta = 0$ and $g=2$. These results then illustrate that the unprecedented large STT-driven DW velocities measured in $\text{Mn}_{4-x}\text{Ni}_x\text{N}$ can be attributed to the magnetization reduction close to the compensation point, together with the large spin polarization of the conduction electrons.

As already mentioned, a reversal of the DW motion direction is observed when crossing the magnetization compensation composition. This behaviour is remarkable, as it is different from the one previously observed in the case of ferrimagnetic samples in the presence of DMI, where chiral Néel walls driven to motion by SHE-SOT move in the same direction below and above the compensation temperature^{19,20}. In order to shed light on this result, we carried out *ab initio* calculations.

***Ab initio* calculations**

First principles calculations were performed in the framework of density functional theory (DFT) using spin polarized relativistic Korringa-Kohn-Rostoker (SPR-KKR) and Vienna

Ab Initio Simulation packages^{42–47}. The calculations for Mn_4N were based on the perovskite crystal structure ($Pm\bar{3}m$ space group) with lattice parameter of 3.74 Å and collinear magnetic configuration, as shown in Fig. 1a. The total magnetic moment along the [001] quantization axis was found to be 1 μ_B (Mn I: 3.3 μ_B , Mn II : -0.8 μ_B) in good agreement with previous reports^{48,49}. Ni doping in $\text{Mn}_{4-x}\text{Ni}_x\text{N}$ was taken into account using both the supercell approach and the coherent potential approximation (CPA) as implemented in SPR-KKR code^{50–52} (see Methods for details).

Fig. 4a shows that the calculated total magnetic moment decreases linearly with the Ni concentration, reaches the compensation point and reverses direction with respect to the global quantization axis for $x=0.15$ using the SPR-KKR approach and for $x=0.17$ using the VASP approach. The calculated compensation point is in good agreement with the experimental one. Fig. 4b,c present the projected density of states (PDOS) calculated for the Mn(I) and Mn(II) sites of Mn_4N , while Fig. 4d,e,f show the s-PDOS of Ni substituted at site Mn(I), together with that of the Mn(I) and Mn(II) sites of $\text{Mn}_{3.75}\text{Ni}_{0.25}\text{N}$. These curves show that for both samples (below and above the compensation point) the PDOS at the Fermi level (E_F) is about one order of magnitude larger for the Mn(II) site, with respect to that of the Mn(I) and the Ni sites. Moreover, it is larger for the majority (i.e. parallel to the global quantization axis) than the minority electrons. In summary, this study allows us to conclude that, for film compositions both below and above the compensation point, the spin polarization of the conduction electrons is parallel to the (001) quantization axis and mostly due to the majority carriers in Mn(II) atoms.

Discussion and conclusions

The direction of motion of DWs driven by STT depends on the relative orientations of the conduction electron spin polarization and the net magnetization. According to the *ab initio* calculations, in $\text{Mn}_{4-x}\text{Ni}_x\text{N}$ films with composition x below the compensation point,

the spin polarization and the net magnetization are parallel to the (001) quantization axis (parallel to the Mn(I) moment), so that the DWs are expected to move in the direction of the electron flow. On the other hand, for compositions above the compensation point, the net magnetization changes direction while the spin polarization does not, so that they become anti-parallel. As a consequence, the domain walls are expected to move in the direction opposite to the electron flow, therefore explaining the observed results.

It is interesting to note that in ferrimagnetic systems deposited on a heavy metal, where the motion of chiral Néel walls is driven by SHE-SOT, the DW motion was observed to maintain the same direction when crossing the compensation point^{19,20}. When SHE-SOT is the driving mechanism, the direction of motion is determined by the DW chirality, set by the signs of the Dzyaloshinskii-Moriya interaction and of the spin Hall angle. Since the spin Hall angle only depends on the type of heavy metal underlayer, and the sign of the DMI is not expected to change for a small change of temperature (or composition), the domain wall motion does not change direction when crossing the compensation point. This explains the different behaviour in the two types of samples.

In conclusion, we have investigated $\text{Mn}_{4-x}\text{Ni}_x\text{N}$ ferrimagnetic thin films in which a fine tuning of Ni doping allows adjusting the magnetic compensation temperature around room temperature. Current-driven domain wall velocity measurements were carried out for samples with various Ni content, having net magnetization on either sides of the compensation point. Due to the decrease of their saturation magnetization and the persistence of a strong spin polarization of the conduction electrons, the domain wall mobility was found to strongly increase in films with compositions close to the compensation point. Record domain wall velocities approaching 3000 m/s were observed for relatively low current densities ($J= 1.2 \times 10^{12}$ A/m²). The domain wall mobilities measured for these samples, at room temperature and without the support of an in-plane magnetic field that increases the DW width²¹, are of the same order of magnitude of those observed recently in ferrimagnetic thin films where DWs walls are driven by SHE-SOT^{19,21}.

Remarkably, the domain walls in $\text{Mn}_{4-x}\text{Ni}_x\text{N}$ were observed to have opposite direction of motion for compositions below and above the compensation point: they move in the direction parallel to the electron flow for compositions below the compensation point, and in the opposite direction above the compensation point. Following the results of *ab initio* calculations, this effect is attributed to the opposite relative directions of the net magnetization and the conduction electrons spin polarization for films with compositions on either sides of the compensation composition.

This work shows that although most of the recent efforts have focused on SOT-driven dynamics of domain walls in thin films with DMI, STT appears to be also a very efficient way to drive domain walls, provided that the film has a reduced magnetization (e.g. it is a ferrimagnet close to compensation points) and a strong spin polarization. Our material, composed of abundant elements, and free of critical elements such as Co, rare earths and heavy metals, is a promising candidate for sustainable spintronics applications.

Methods

Sample growth

The magnetic films were deposited on commercial $300\ \mu\text{m}$ STO(100) substrates. The substrates were treated with HF and NH_4F solutions to smoothen the surface and were cleaned to remove any other impurities. 10 nm and 30 nm thick $\text{Mn}_{4-x}\text{Ni}_x\text{N}$ films were then epitaxially grown at 450°C with Mn and Ni atoms coming from the solid sources of high temperature Knudsen cells and using a radio-frequency nitrogen plasma source. The growth conditions were optimised at 1 nm/min with a N_2 gas flow of $0.9\ \text{cm}^3/\text{min}$ with 4.1×10^{-3} Pa pressure in the chamber. To prevent further oxidation, the thin films were then capped in-situ with 3 nm of SiO_2 using a sputtering gun using argon plasma source.

Ab initio calculations

The Vienna ab initio simulation package (VASP)⁴²⁻⁴⁴ was used for structure optimization, where the electron-core interactions are described by the projector augmented wave method for the potentials⁴⁵, and the exchange correlation energy is calculated within the generalized gradient approximation (GGA) of the Perdew-Burke Ernzerhof form^{46,47}. The cutoff energies for the plane wave basis set used to expand the Kohn-Sham orbitals were 500 eV for all calculations. Structural relaxations and total energy calculations were performed ensuring that the Hellmann-Feynman forces acting on ions were less than 10^{-2} N. Using a $44 \times 44 \times 44 \text{ \AA}^{-1}$ k-mesh the obtained bulk lattice constant of Mn_4N after full lattice relaxation was 3.74 Å. Ni doping in $\text{Mn}_{4-x}\text{Ni}_x\text{N}$ were taken into account using the supercell approach, where we replaced an atom of Mn I by Ni in $1 \times 1 \times 4$ and $1 \times 1 \times 8$ unit cell to model $x= 0.25$ and $x= 0.125$, respectively. To verify the supercell approach we also calculated the effect of Ni doping in $\text{Mn}_{4-x}\text{Ni}_x\text{N}$ using the coherent potential approximation as implemented in SPR-KKR code.

Domain wall velocity measurements

Mn_4N and $\text{Mn}_{4-x}\text{Ni}_x\text{N}$ thin films were patterned with standard e-beam lithography and Ar milling to obtain Hall bars of different sizes and $1 \text{ }\mu\text{m}$ wide and $20 \mu\text{m}$ long nanowires. The electrodes consisted of a Ti/Au/Ti film deposited on top of the microstructures as a contact material, and were processed with standard optical lithography and ion etching. Polar magneto-optical Kerr microscopy was used to image the magnetic structure. Strong out-of-plane magnetic field pulses were used to nucleate reverse domains in the nucleation pads and to inject the domain walls into the nanowires. The domain walls were displaced by injecting both positive and negative DC current pulses. The current pulses were obtained using a generator providing voltage pulses of amplitude up to 80 V and width down to 1 ns. The shape of the pulses was captured and stored using an oscilloscope. The domain wall displacement during the application of the positive and negative current pulses was derived

from the differential MOKE images. The DW displacements from the different wires were averaged to obtain a precise estimation of the domain wall velocity v . This was obtained by dividing averaged displacement by the averaged full width at half maximum (FWHM) of the pulse widths multiplied by the number of pulses: $v = \Delta x / (pw)$, where Δx is the averaged displacement of the domain wall, p is the number of current pulses and w is the FWHM of the current pulses, calculated by fitting it with an asymmetric double sigmoidal function. From the peak values obtained from this fitting and their variation with respect to the original pulses, the current density was calculated with an error bar. This process was repeated for all the different current densities to obtain the velocity curves vs. current density, for all the $\text{Mn}_{4-x}\text{Ni}_x\text{N}$ thin films.

All the DW velocity measurements were limited to current densities below $J=1.2 \times 10^{12}$ A/m², since above this current density the Joule heating causes the proliferation of nucleated domains. The effect of Joule heating is particularly important as the Ni concentration increases, where an increase in the resistivity was measured. This heating effect may be reduced using thinner and narrower nanowires.

Anomalous Hall effect (AHE) measurements

AHE measurements were performed on Hall bars of $10\mu\text{m}$ width for most of the samples. Some of the AHE measurements were also performed using the Van der Pauw method in smaller $0.5 \times 0.5 \text{ cm}^2$ continuous films.

Acknowledgements

We acknowledge Dr. Isogami from NIMS in Japan for the measurement of the damping factor. The devices were prepared in PTA platform from Grenoble, with partial support from the French RENATECH network. We acknowledge funding from IDEX-DOMINO project and JSPS KAKENHI (No. 19KK0104 and 19K21954). J.P.G. acknowledges the

European Union’s Horizon 2020 research and innovation program under Marie Skłodowska-Curie Grant Agreement No. 754303 and the support from the Laboratoire d’excellence LANEF in Grenoble (ANR-10-LABX-0051).

Author Information

Corresponding Authors

* E-mail: stefania.pizzini@neel.cnrs.fr

* E-mail: laurent.vila@cea.fr

Author Contributions

L.V., J.P.A., T.S. and S.P. managed the project and conceived the experiments. S.G., T.G., T.O., T.H., and H.M. prepared the samples. S.G. and T.G. realized the transport measurements. S.G. and T.G. performed the domain wall dynamics measurements with the guidance of S.P. H.O. made the TEM measurements. J.V. and S.G. performed the magnetization measurements. L.V., T. G. and S.G. patterned the samples by electron beam lithography. A. H. and M.C. made the ab initio calculations. S.P., J.P. A. and S.G. wrote the manuscript. All the authors discussed the results and commented on the manuscript.

References

- (1) Berger, L. Low-field magnetoresistance and domain drag in ferromagnets. *Journal of Applied Physics* **1978**, *49*, 2156–2161
- (2) Parkin, S.; Yang, S.-H. Memory on the racetrack. *Nature Nanotechnology* **2015**, *10*, 195–198

- (3) Brataas, A.; Kent, A. D.; Ohno, H. Current-induced torques in magnetic materials. *Nature Materials* **2012**, *11*, 372–381
- (4) Nikonov, D. E.; Bourianoff, G. I.; Ghani, T. Proposal of a Spin Torque Majority Gate Logic. *IEEE Electron Device Letters* **2011**, *32*, 1128–1130
- (5) Vaysset, A.; Manfrini, M.; Nikonov, D. E.; Manipatruni, S.; Young, I. A.; Pourtois, G.; Radu, I. P.; Thean, A. Toward error-free scaled spin torque majority gates. *AIP Advances* **2016**, *6*, 065304
- (6) Allwood, D. A. Submicrometer Ferromagnetic NOT Gate and Shift Register. *Science* **2002**, *296*, 2003–2006
- (7) Currivan, J. A.; Youngman Jang,; Mascaro, M. D.; Baldo, M. A.; Ross, C. A. Low Energy Magnetic Domain Wall Logic in Short, Narrow, Ferromagnetic Wires. *IEEE Magnetism Letters* **2012**, *3*, 3000104–3000104
- (8) Currivan-Incorvia, J. A.; Siddiqui, S.; Dutta, S.; Everts, E. R.; Zhang, J.; Bono, D.; Ross, C. A.; Baldo, M. A. Logic circuit prototypes for three-terminal magnetic tunnel junctions with mobile domain walls. *Nature Communications* **2016**, *7*, 10275
- (9) Luo, Z.; Hrabec, A.; Dao, T. P.; Sala, G.; Finizio, S.; Feng, J.; Mayr, S.; Raabe, J.; Gambardella, P.; Heyderman, L. J. Current-driven magnetic domain-wall logic. *Nature* **2020**, *579*, 214–218
- (10) Slonczewski, J. Current-driven excitation of magnetic multilayers. *Journal of Magnetism and Magnetic Materials* **1996**, *159*, L1–L7
- (11) Freitas, P. P.; Berger, L. Observation of s - d exchange force between domain walls and electric current in very thin Permalloy films. *Journal of Applied Physics* **1985**, *57*, 1266–1269

- (12) Grollier, J.; Boulenc, P.; Cros, V.; Hamzić, A.; Vaurès, A.; Fert, A.; Faini, G. Switching a spin valve back and forth by current-induced domain wall motion. *Applied Physics Letters* **2003**, *83*, 509–511
- (13) Yamaguchi, A.; Ono, T.; Nasu, S.; Miyake, K.; Mibu, K.; Shinjo, T. Real-Space Observation of Current-Driven Domain Wall Motion in Submicron Magnetic Wires. *Physical Review Letters* **2004**, *92*, 077205
- (14) Khvalkovskiy, A. V.; Zvezdin, K. A.; Gorbunov, Y. V.; Cros, V.; Grollier, J.; Fert, A.; Zvezdin, A. K. High Domain Wall Velocities due to Spin Currents Perpendicular to the Plane. *Physical Review Letters* **2009**, *102*, 067206
- (15) Haazen, P. P. J.; Murè, E.; Franken, J. H.; Lavrijsen, R.; Swagten, H. J. M.; Koopmans, B. Domain wall depinning governed by the spin Hall effect. *Nature Materials* **2013**, *12*, 299–303
- (16) Emori, S.; Bauer, U.; Ahn, S.-M.; Martinez, E.; Beach, G. *Nat. Mater.* **2013**, *12*, 611
- (17) Ryu, K.-S.; Thomas, L.; Yang, S.-H.; Parkin, S. Chiral spin torque at magnetic domain walls. *Nature Nanotechnology* **2013**, *8*, 527
- (18) Kim, K.-J.; Kim, S. K.; Hirata, Y.; Oh, S.-H.; Tono, T.; Kim, D.-H.; Okuno, T.; Ham, W. S.; Kim, S.; Go, G.; Tserkovnyak, Y.; Tsukamoto, A.; Moriyama, T.; Lee, K.-J.; Ono, T. Fast domain wall motion in the vicinity of the angular momentum compensation temperature of ferrimagnets. *Nature Materials* **2017**, *16*, 1187
- (19) Caretta, L. et al. Fast current-driven domain walls and small skyrmions in a compensated ferrimagnet. *Nature Nanotechnology* **2018**, *13*, 1154–1160
- (20) Siddiqui, S. A.; Han, J.; Finley, J. T.; Ross, C. A.; Liu, L. Current-Induced Domain Wall Motion in a Compensated Ferrimagnet. *Physical Review Letters* **2018**, *121*, 057701

- (21) Caretta, L.; Oh, S.-H.; Fakhrol, T.; Lee, D.-K.; Lee, B. H.; Kim, S. K.; Ross, C. A.; Lee, K.-J.; Beach, G. S. D. Relativistic kinematics of a magnetic soliton. *Science* **2020**, *370*, 1438
- (22) Takei, W. J.; Shirane, G.; Frazer, B. C. Magnetic Structure of Mn_4N . *Physical Review* **1960**, *119*, 122–126
- (23) Takei, W. J.; Heikes, R. R.; Shirane, G. Magnetic Structure of Mn_4N -Type Compounds. *Physical Review* **1962**, *125*, 1893–1897
- (24) Mekata, M. Magnetic Study on Mn_4N and its Related Compounds. *Journal of the Physical Society of Japan* **1962**, *17*, 796–803
- (25) Fruchart, D.; Givord, D.; Convert, P.; l’Heritier, P.; Senateur, J. P. The non-collinear component in the magnetic structure of Mn_4N . *Journal of Physics F: Metal Physics* **1979**, *9*, 2431–2437
- (26) Ching, K. M.; Chang, W. D.; Chin, T. S.; Duh, J. G.; Ku, H. C. Anomalous perpendicular magnetoanisotropy in Mn_4N films on Si(100). *Journal of Applied Physics* **1994**, *76*, 6582–6584
- (27) Yasutomi, Y.; Ito, K.; Sanai, T.; Toko, K.; Suemasu, T. Perpendicular magnetic anisotropy of Mn_4N films on $\text{MgO}(001)$ and $\text{SrTiO}_3(001)$ substrates. *Journal of Applied Physics* **2014**, *115*, 17A935
- (28) Kabara, K.; Tsunoda, M. Perpendicular magnetic anisotropy of Mn_4N films fabricated by reactive sputtering method. *Journal of Applied Physics* **2015**, *117*, 17B512
- (29) Shen, X.; Chikamatsu, A.; Shigematsu, K.; Hirose, Y.; Fukumura, T.; Hasegawa, T. Metallic transport and large anomalous Hall effect at room temperature in ferrimagnetic Mn_4N epitaxial thin film. *Applied Physics Letters* **2014**, *105*, 072410

- (30) Meng, M.; Wu, S. X.; Ren, L. Z.; Zhou, W. Q.; Wang, Y. J.; Wang, G. L.; Li, S. W. Extrinsic anomalous Hall effect in epitaxial Mn_4N films. *Applied Physics Letters* **2015**, *106*, 032407
- (31) Ito, K.; Yasutomi, Y.; Kabara, K.; Gushi, T.; Higashikozono, S.; Toko, K.; Tsunoda, M.; Suemasu, T. Perpendicular magnetic anisotropy in $\text{Co}_x\text{Mn}_{4-x}\text{N}$ ($x = 0$ and 0.2) epitaxial films and possibility of tetragonal Mn_4N phase. *AIP Advances* **2016**, *6*, 056201
- (32) Dhar, S.; Brandt, O.; Ploog, K. H. Ferrimagnetic $\text{Mn}_4\text{N}(111)$ layers grown on $6\text{H-SiC}(0001)$ and $\text{GaN}(0001)$ by reactive molecular-beam epitaxy. *Applied Physics Letters* **2005**, *86*, 112504
- (33) Gushi, T.; Vila, L.; Fruchart, O.; Marty, A.; Pizzini, S.; Vogel, J.; Takata, F.; Anzai, A.; Toko, K.; Suemasu, T.; Attané, J.-P. Millimeter-sized magnetic domains in perpendicularly magnetized ferrimagnetic Mn_4N thin films grown on SrTiO_3 . *Japanese Journal of Applied Physics* **2018**, *57*, 120310
- (34) Hirose, T.; Komori, T.; Gushi, T.; Toko, K.; Suemasu, T. Perpendicular magnetic anisotropy in ferrimagnetic Mn_4N films grown on $(\text{LaAlO}_3)_{0.3}(\text{Sr}_2\text{TaAlO}_6)_{0.7}(0\ 0\ 1)$ substrates by molecular beam epitaxy. *Journal of Crystal Growth* **2020**, *535*, 125566
- (35) Gushi, T.; Jovičević Klug, M.; Peña Garcia, J.; Ghosh, S.; Attané, J.-P.; Okuno, H.; Fruchart, O.; Vogel, J.; Suemasu, T.; Pizzini, S.; Vila, L. Large Current Driven Domain Wall Mobility and Gate Tuning of Coercivity in Ferrimagnetic Mn_4N Thin Films. *Nano Letters* **2019**, *19*, 8716–8723
- (36) Komori, T.; Hirose, T.; Gushi, T.; Toko, K.; Hanashima, C.; Vila, L.; Attané, J.-P.; Amemiya, K.; Suemasu, T. Magnetic reversal in rare-earth free $\text{Mn}_{4-x}\text{Ni}_x\text{N}$ epitaxial films below and above Ni composition needed for magnetic compensation around room temperature. *Journal of Applied Physics* **2020**, *127*, 043903

- (37) Komori, T.; Gushi, T.; Anzai, A.; Vila, L.; Attané, J.-P.; Pizzini, S.; Vogel, J.; Isogami, S.; Toko, K.; Suemasu, T. Magnetic and magneto-transport properties of Mn_4N thin films by Ni substitution and their possibility of magnetic compensation. *Journal of Applied Physics* **2019**, *125*, 213902
- (38) Thiaville, A.; Nakatani, Y.; Miltat, J.; Suzuki, Y. Micromagnetic understanding of current-driven domain wall motion in patterned nanowires. *Europhysics Letters (EPL)* **2005**, *69*, 990–996
- (39) Mougín, A.; Cormier, M.; Adam, J. P.; Metaxas, P. J.; Ferré, J. Domain wall mobility, stability and Walker breakdown in magnetic nanowires. *Europhysics Letters (EPL)* **2007**, *78*, 57007
- (40) Zhang, S.; Li, Z. Roles of Nonequilibrium Conduction Electrons on the Magnetization Dynamics of Ferromagnets. *Phys. Rev. Lett.* **2004**, *93*, 127204
- (41) Malinowski, G.; Boulle, O.; Kläui, M. Current-induced domain wall motion in nanoscale ferromagnetic elements. *Journal of Physics D: Applied Physics* **2011**, *44*, 384005
- (42) Kresse, G.; Hafner, J. *Ab initio* molecular dynamics for liquid metals. *Physical Review B* **1993**, *47*, 558–561
- (43) Kresse, G.; Furthmüller, J. Efficiency of *ab-initio* total energy calculations for metals and semiconductors using a plane-wave basis set. *Computational Materials Science* **1996**, *6*, 15–50
- (44) Kresse, G.; Furthmüller, J. Efficient iterative schemes for *ab initio* total-energy calculations using a plane-wave basis set. *Physical Review B* **1996**, *54*, 11169–11186
- (45) Blöchl, P. E. Projector augmented-wave method. *Physical Review B* **1994**, *50*, 17953–17979

- (46) Perdew, J. P.; Burke, K.; Ernzerhof, M. Generalized Gradient Approximation Made Simple. *Physical Review Letters* **1996**, *77*, 3865–3868
- (47) Kresse, G.; Joubert, D. From ultrasoft pseudopotentials to the projector augmented-wave method. *Physical Review B* **1999**, *59*, 1758–1775
- (48) Meinert, M. Exchange interactions and Curie temperatures of the tetrametal nitrides Cr₄N, Mn₄N, Fe₄N, Co₄N, and Ni₄N. *Journal of Physics: Condensed Matter* **2016**, *28*, 056006
- (49) Isogami, S.; Masuda, K.; Miura, Y. Contributions of magnetic structure and nitrogen to perpendicular magnetocrystalline anisotropy in antiperovskite ϵ Mn₄N. *Physical Review Materials* **2020**, *4*, 014406
- (50) Ebert, H.; Koedderitzsch, D.; Minar, J. Calculating condensed matter properties using the KKR-Green's function method-recent developments and applications. *Reports on Progress in Physics* **2011**, *74*, 096501
- (51) Ebert, H.; Braun, J.; Koedderitzsch, D.; Mankovsky, S. Fully relativistic multiple scattering calculations for general potentials. *Physical Review B* **2016**, *93*, 075145
- (52) Ebert, H. The Munich SPR-KKR package. [http://olymp.cup.uni-muenchen.de/ak/ebert/SPRKKRversion6.3\(2012\).](http://olymp.cup.uni-muenchen.de/ak/ebert/SPRKKRversion6.3(2012).)

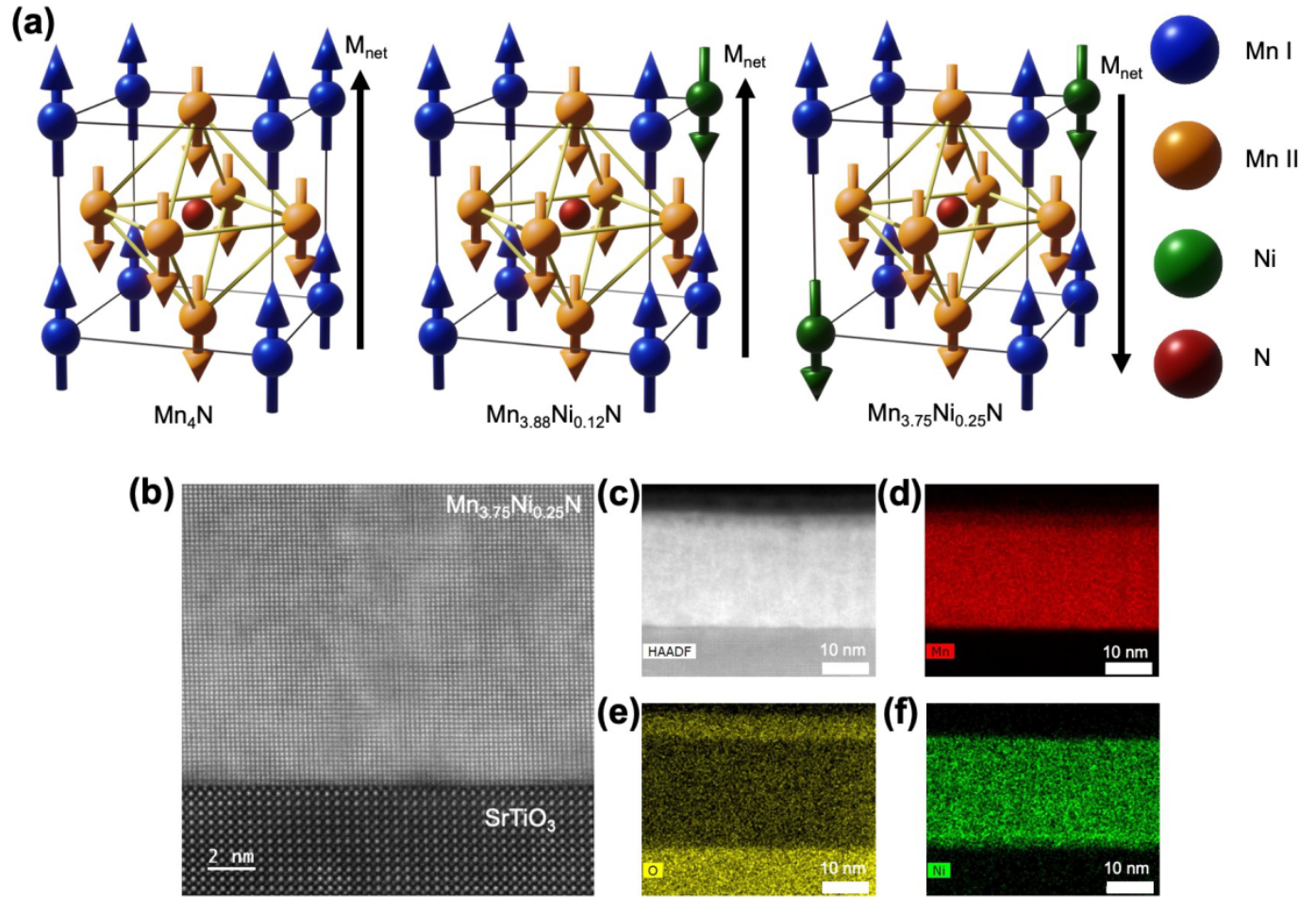


Fig. 1: (a) Schematics of the anti-perovskite crystal structure of Mn_4N (left), showing the substitution of the Mn(I) site atoms (in blue) with Ni atoms, to model $Mn_{1-x}Ni_xN$ (middle and right). Mn(II) atoms are shown in orange, Ni atoms in green and nitrogen atoms in red. Mn(I) magnetic moments are parallel to the [001] quantization axis. The net magnetization decreases when increasing the Ni concentration, and after crossing the magnetic compensation point the direction of the net magnetic moment is reversed. (b) High resolution STEM image of a 30 nm $Mn_{3.75}Ni_{0.25}N$ thin film deposited onto a STO substrate. (c) HAADFSTEM image of the full thin film with the capping layer of 3 nm SiO_2 and associated EDX elemental map of Mn (d), O (e) and Ni (f).

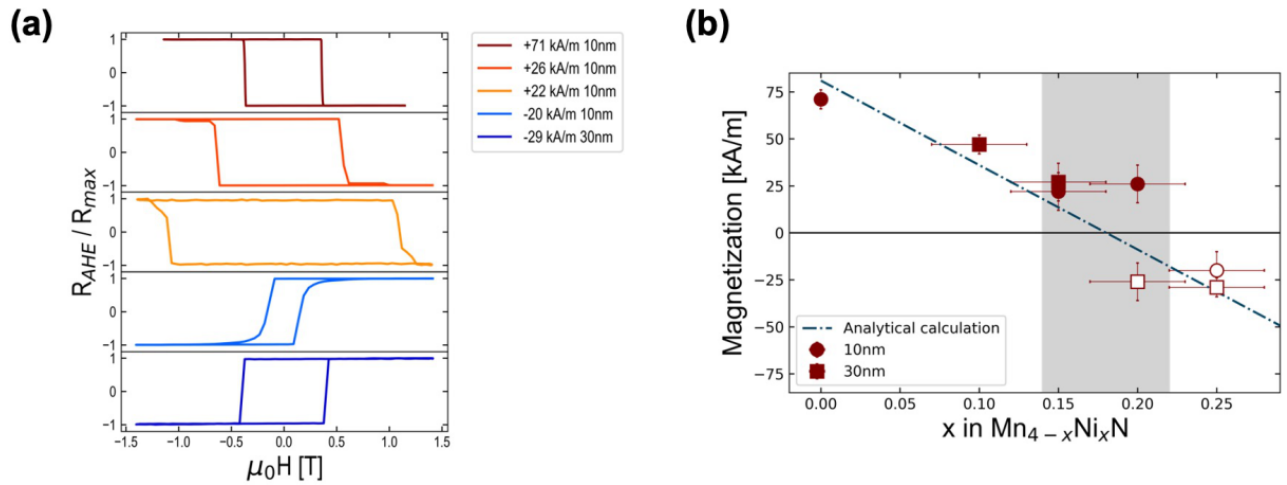


Fig. 2: (a) Anomalous Hall effect curves measured for thin films with different Ni concentrations ($x=0$ (10 nm), 0.15(10 nm), 0.2(10 nm), 0.25(10 nm) and 0.25(30 nm)). The sign of the Hall angle changes from negative to positive when crossing the magnetic compensation point between $x=0.15$ and $x=0.25$, indicating the change of direction of the net magnetization. The corresponding net magnetization values measured by VSM-SQUID are reported in the caption. (b) Spontaneous magnetization versus nominal Ni concentration x , measured for the $Mn_{4-x}Ni_xN$ thin films by VSM-SQUID. The sign of the net magnetization is obtained from the sign of the AHE angle. The shaded area indicates the spread of the observed deviation of the Ni content x at the compensation point, with respect to the nominal value. The dotted line shows the magnetization obtained analytically.

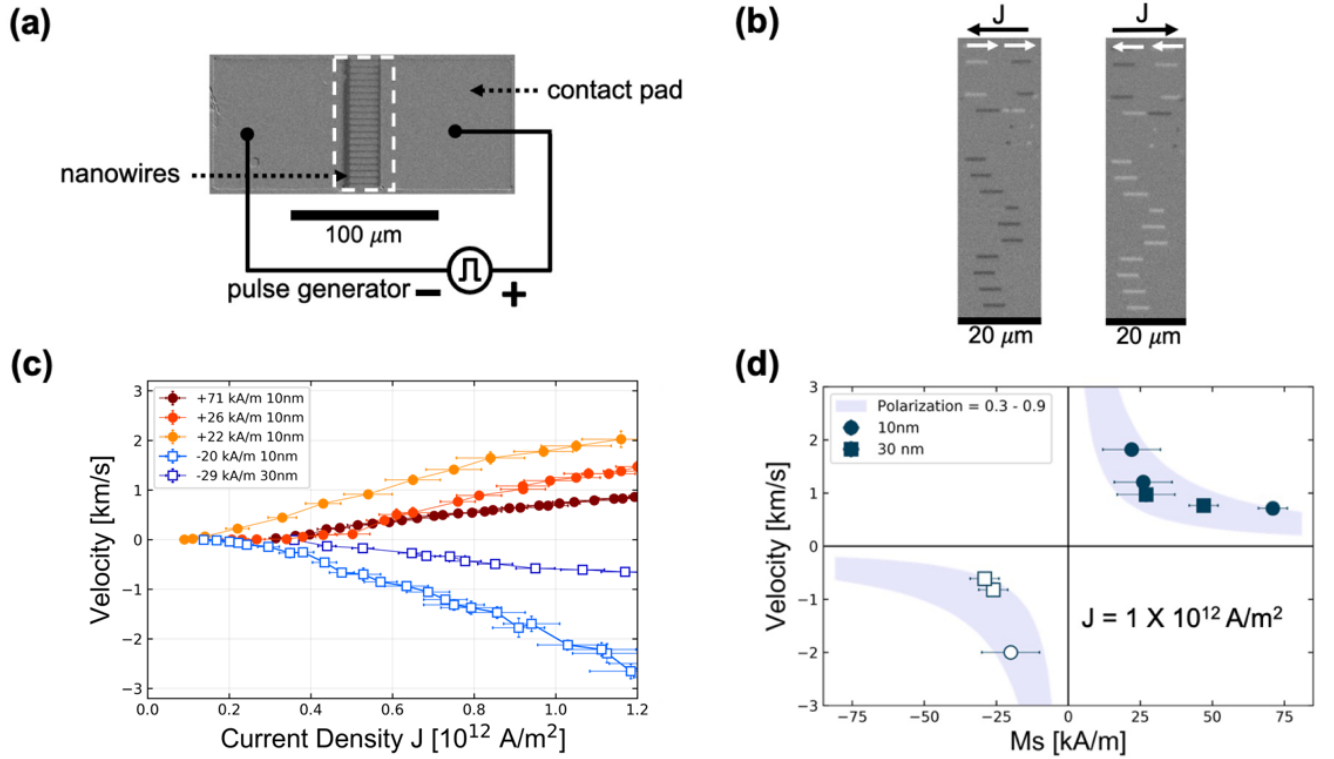


Fig. 3: (a) Sketch of the devices fabricated for the measurement of domain wall dynamics, showing twenty parallel nanowires where DWs are driven by polarized current pulses, together with the contact pads from which the DWs are injected. (b) Differential polar MOKE images, showing the displacement of domain walls during the application of a negative (left) and positive (right) current pulses. The white arrows indicate the DW displacement. In this device with composition below the compensation point, the DWs move in the direction of the electron flow. (c) Domain wall speed versus current density for $\text{Mn}_{4-x}\text{Ni}_x\text{N}$ films with different Ni concentration on either sides of the compensation point. $M_S=71$ kA/m corresponds to Mn_4N ($x=0$). The filled/empty symbols show the velocity below/above the compensation point: the DW direction of motion changes sign when crossing the compensation point. (d) Domain wall velocity versus net magnetization M_S measured for $J=1 \times 10^{12}$ A/m². The graph shows the divergence of the velocity when the compensation point is approached. The shaded area delimits the calculated velocities for spin polarization values between 0.3 and 0.9.

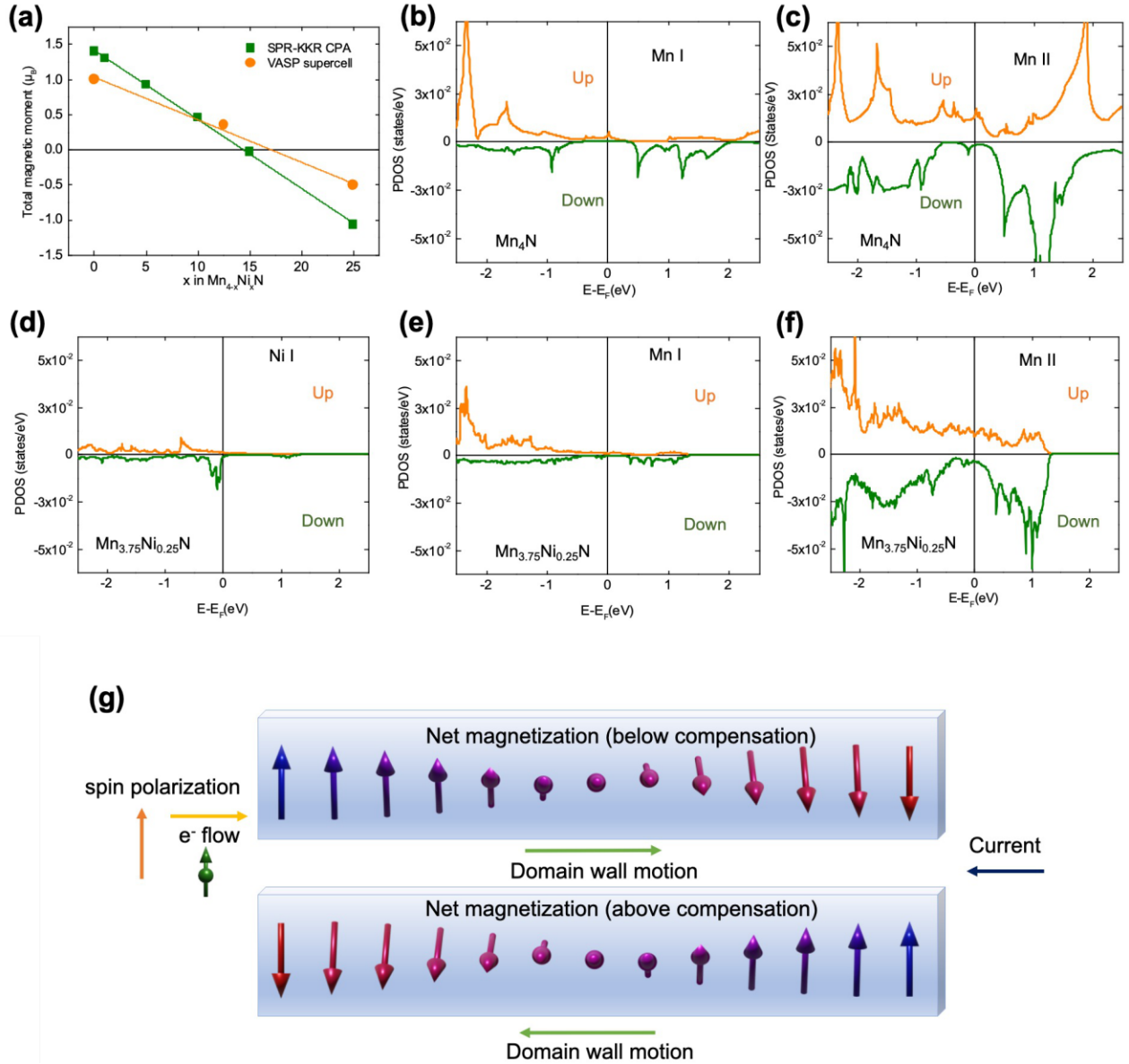


Fig. 4: (a) Ab initio calculation of magnetic moment versus Ni concentration showing a change in the net magnetization direction around $x=0.15$. (b) & (c) s-orbital PDOS of sites Mn(I) and Mn(II) of Mn_4N . The polarization direction at the Fermi level is "up" for both atoms while a much larger PDOS, determining the conduction electron carriers, is obtained for the Mn(II) site. (d), (e) & (f) s-orbital PDOS of Ni, Mn(I) and Mn(II) in $Mn_{3.75}Ni_{0.25}N$. The polarization direction at the Fermi level remains "up" for all the atoms. (g) Sketch of a Bloch domain wall with the individual net magnetic moments, for a sample below/above the compensation point (top/bottom). The orange arrow indicates the direction of the spin polarization, that stays constant below and above the compensation point. The yellow line indicates the direction of the spin polarized electron flow. Since the spin polarization direction is constant, while the net magnetization direction changes, the spin-transfer torque pushes the DW in opposite directions below and above the compensation.